### Title

A diverse group of echogenic particles observed with a broadband, high frequency echosounder




### Journal

ICES Journal of Marine Science, 75(2)

### ISSN

1054-3139



### Authors

Briseño-Avena, Christian
Franks, Peter JS
Roberts, Paul LD
et al.



### Publication Date

2018-03-01

### DOI

10.1093/icesjms/fsx171

Peer reviewed

ICES Journal of Marine Science

ICES Journal of Marine Science (2018), 75(2), 471–482. doi:10.1093/icesjms/fsx171



## Food for Thought

# A diverse group of *echogenic* particles observed with a broadband, high frequency echosounder

Christian Briseño-Avena[1,2]*, Peter J. S. Franks[2], Paul L. D. Roberts[3], and Jules S. Jaffe[3]

[1]*Hatfield Marine Science Center, Oregon State University, 2030 SE Marine Science Drive, Newport, OR 97365, USA*
[2]*Integrative Oceanography Division, Scripps Institution of Oceanography, University of California, San Diego, 9500 Gilman Drive, La Jolla, CA 92093, USA*
[3]*Marine Physical Laboratory, Scripps Institution of Oceanography, University of California, San Diego, 9500 Gilman Drive, La Jolla, CA 92093, USA*

**Corresponding author: tel: +1 (541) 867-0419; fax: +1 (541) 867-0138; e-mail: brisenoc@oregonstate.edu*

Briseño-Avena, C., Franks, P. J. S., Roberts, P. L. D., and Jaffe, J. S. A diverse group of *echogenic* particles observed with a broadband, high frequency echosounder. – ICES Journal of Marine Science, 75: 471–482.

Received 19 December 2016; revised 3 August 2017; accepted 4 August 2017; advance access publication 18 September 2017.

In 1980, Holliday and Pieper stated: "Most sound scattering in the ocean volume can be traced to a biotic origin." However, most of the bioacoustics research in the past three decades has focused on only a few groups of organisms. Targets such as small gelatinous organisms, marine snow, and phytoplankton, e.g. have been generally to be considered relatively transparent to acoustic waves due to their sizes and relatively low sound speed and density contrasts relative to seawater. However, using a broadband system (ZOOPS-O$^2$) we found that these targets contributed significantly to acoustic returns in the 1.5–2.5 MHz frequency range. Given that phytoplankton and marine snow layers are ubiquitous features of coastal regions; this works suggests that they should be considered as potential sources of backscatter in biological acoustic surveys.

**Keywords:** broadband echosounder, high frequency, marine snow, phytoplankton, stereoscopic, zooplankton.

## Introduction

There is a continued interest in understanding the sources of oceanic backscatter and the use of echosounders to estimate the abundances and distributions of marine organisms. Using acoustic methods to understand the distributions of biological acoustic scatterers in the water column requires knowledge of the acoustic properties of the targets. Although several ground-truthing experiments (i.e. inter-method comparisons) and models have concentrated on understanding of the acoustic properties and detection of fishes, e.g. relatively little effort has been focused on planktonic organisms. Plankton-oriented studies have been carried out in laboratory settings, through *in situ* observations, modelling efforts, or combinations of these (e.g. Greenlaw, 1977; Holiday and Pieper, 1980; Richter, 1985; Demer and Martin, 1995; Martin *et al.*, 1996; Stanton *et al.*, 1996; Jaffe *et al.*, 1988; Lawson *et al.*, 2004; Briseño-Avena *et al.*, 2015). However, there are still significant gaps in our knowledge. Data from the latest generation of broadband sonars present new opportunities for acoustical investigations of plankton (Lavery *et al.*, 2010; Trenkel *et al.*, 2016). Such investigations require a thorough understanding of the capabilities and limitations of such systems.

Though water is relatively transparent to many acoustic wavelengths, it is relatively opaque to most of the electromagnetic spectrum. Aquatic and fisheries ecologists have therefore favored acoustical methods over optical imaging to conduct large-scale biological surveys of zooplankton and fish assemblages (Fernandes *et al.*, 2002). Though the sensing capability, fast acquisition, and almost real-time processing of acoustical data give acoustical methods an advantage over optical technologies, classification of acoustic target returns can be ambiguous. In contrast to sound, light is strongly attenuated by water, limiting the working range of underwater optical imaging. However, while optical imaging methods lack long-range capabilities (with the exception of oligotrophic waters with low turbidity) they are capable of

generating detailed images of targets, commonly allowing identification down to genus and often to species; coarse taxonomic identification (e.g. copepod, hydromedusa, ctenophore, chaetognath, appendicularian, etc.) is almost always possible.

Historically, narrowband acoustic systems working at discrete frequencies have been at the forefront of acoustical methods (Stanton, 2012 and references therein; Fornshell and Tesei, 2013). However, determining the identity of the targets insonified by such tools has been a major challenge. New developments in broadband acoustic sensors and signal processing have begun to give us new insights into the acoustical properties of planktonic organisms. With a few exceptions in higher latitudes, most marine ecosystems are species rich (e.g. De Monte *et al.*, 2013), with a high diversity of species, body shapes, sizes, compositions, and behaviours. In such regions acoustical methods are at a disadvantage when compared with optical ones: while it is possible to visually distinguish among planktonic taxa, it is difficult to acoustically differentiate even the most basic forms with current signal-processing methods (Fielding *et al.*, 2004) and the use of narrowband systems.

Ground-truthing exercises are by far the best and most direct method to aid in the interpretation of acoustic data. Comparing acoustic data to net-derived and optic-derived estimates of abundance and/or biomass is the most common approach (e.g. Wiebe *et al.*, 1996; Benfield *et al.*, 1998; Sutor *et al.*, 2005; Lara-Lopez and Neira, 2008; Powell and Ohman, 2012). However, fragile organisms such as jellyfish (e.g. hydromedusae, narcomedusae, medusae), ctenophores, siphonophores, doliolids, and appendicularians are often severely damaged by nets, making it difficult to fully account for them during acoustic-net comparisons. Furthermore, particles (i.e. marine snow) and organisms such as phytoplankton are not sampled by nets targeting zooplankton. Because the goal has generally been to sample zooplankton, other organisms and particles are typically unaccounted for during traditional ground-truthing experiments, despite their conspicuous presence in rich, productive regions of the ocean.

One possible justification for ignoring such targets is that they have been thought to make relatively small contributions to acoustic backscatter at commonly used frequencies. To explore the validity of this assumption, this work investigates the acoustic reflectivity of these often-ignored organisms and particles at the ultrasonic frequencies of 1.5–2.5 MHz.

The idea of phytoplankton and marine snow contributing to acoustic returns is not new; references as far back as the 1950s (Cushing *et al.*, 1956) mention this possibility. After a gap of almost four decades, the idea of such targets contributing to acoustic returns re-surfaced in a report by Anoshkin and Goncharov (1993). Since then, there have been a few efforts to quantify the acoustic reflectance of phytoplankton (Selivanovsky *et al.*, 1996; Bok *et al.*, 2010, 2013), and large (9.6–61 cm umbrella diameter) gelatinous organisms (Mutlu, 1996; Brierley *et al.*, 2005; Warren and Smith, 2007, Weibe *et al.*, 2010) in laboratory settings. However, no attempts have focused on the potential acoustic reflectance of phytoplankton and marine snow in the field. Because of their microscopic size, fragile composition, and patchy distribution, these targets have not been studied in underwater acoustical research and perhaps more importantly, in the interpretation of high-frequency acoustic survey data.

Thin phytoplankton layers are ubiquitous features of coastal regions, extending over kilometers and persisting from hours to several days. Their thickness ranges from tens of centimeters to a few meters as documented in a variety of marine environments (e.g. Cowles *et al.*, 1998; McManus *et al.*, 2003). Phytoplanktons have usually been considered transparent to acoustic waves, and thus ignored as potential acoustic reflectors. Recently, however, Timmerman *et al.* (2014) suggested that a layer of large diatom flocculates (~2 cm in diameter) was detected with a narrowband sonar (200 kHz). The authors, however, could not refute the hypothesis that the high acoustic returns were caused by the presence of oxygen bubbles.

Marine snow layers are common features of coastal waters (Alldredge and Silver, 1988; Alldredge *et al.*, 2002), occurring in both surface waters, and—unlike phytoplankton—at depths well below the euphotic zone (e.g. Ransom *et al.*, 1998). However, little work has been conducted on acoustic estimates of these abundant and densely aggregated particles, though there are anecdotal references in the acoustical literature (e.g. Anoshkin and Goncharov, 1993).

One approach to understanding the sources of reflected sound is to combine optical imaging and acoustical methods, orienting the sensors so that a common volume is observed by both modalities, such as the ZOOPS-$O^2$ system that measures the acoustic reflectivity of targets *in situ* with coincident optical determination of taxa, size, and orientation (Briseño-Avena *et al.*, 2015). Here, we use data acquired by that system to estimate the acoustic reflectivity of phytoplankton, marine snow, and small gelatinous organisms (350 μm–24 mm), as well as the widely accepted strong scatterers such as crustaceans.

## Material and methods

### ZOOPS-$O^2$ system description

ZOOPS-$O^2$ is a broadband, ultra high-frequency (1.5–2.5 MHz) system that combines an instrument to measure the *in situ* acoustic reflectivity of individual targets (ZOOPlankton Sonar: ZOOPS) with two cameras (O-Cam 1 and O-Cam 2: $O^2$) giving concurrent stereo visual images (later referred to as "image pairs") of the targets reflecting the sound. We refer the reader to Briseño-Avena *et al.* (2015) for a full system description. In the following sections we give a brief explanation of the platform to add information relevant to this work that has not been discussed in detail in previous publications.

Acoustic target strength (TS) values for the ZOOPS-$O^2$ system are given as broadband target strength (BTS), and reported for each *individual* target. Unlike the common TS measurement used for discrete-frequency, narrowband systems, the BTS represents the intensity of the returned energy weighted over the 1 MHz bandwidth of the chirp:

$$\mathrm{BTS} = 10 log_{10}\left(\frac{y_{\mathrm{bs}}}{y_{\mathrm{cal}}}\right) - 58.1 \text{ dB } re \text{ 1 } m, \qquad (1)$$

where $y_{\mathrm{bs}}$ is the magnitude-squared of the compressed pulse of the echo from a target, and $y_{\mathrm{cal}}$ is the magnitude-squared of the first reflection from the echo of a calibration sphere (Briseño-Avena *et al.*, 2015).

Five volumes are sampled by individual and combined components of ZOOPS-$O^2$ (Figure 1). The transducer acoustic beam insonifies 1 L of water over a range of 0.65–1.22 m (tall polygon in Figure 1a, and long, thin cylinder in Figure 1b), with an ability to resolve targets that are farther than 1.5 mm apart in range. This range resolution results from the fact that we use an envelope on the chirp waveform that reduces the usable bandwidth of

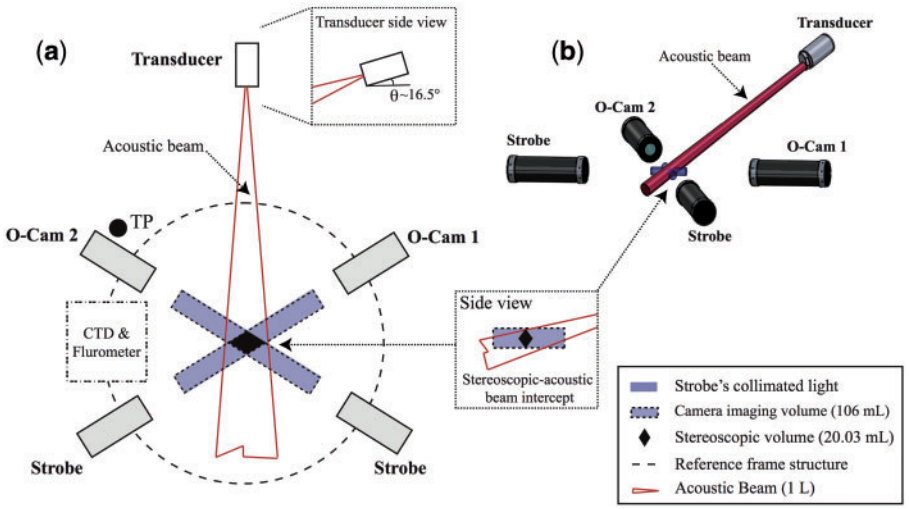


**Figure 1.** Schematic representation of ZOOPS-O$^2$ showing the relative position of the stereoscopic camera system, transducer, and ancillary sensors (CTD, Fluorometer). Modified version of Figure 5 from Briseño-Avena *et al.* (2015) to highlight components relevant to this work—the three different volume estimates used in the present analysis: individual camera imaging volumes, stereoscopic volume, and insonified (acoustic beam) volume.

the system to roughly 500 kHz. Each camera has an individual imaging volume of 106 mL (dashed rectangles in Figure 1a, and small cylinders crossing the acoustic beam in Figure 1b). The stereoscopic volume—the intersection of the two camera imaging volumes (black diamond in Figure 1a)—has an effective sampling volume of 20.03 mL. The entire stereoscopically imaged volume is contained within the acoustic beam at acoustic ranges between 0.84 and 0.88 m. Finally, the acoustic beam (side-view inset pointing to Figures 1a and b) intersecting the stereoscopic volumes at ranges 0.84–0.88 m (bean diameter ranging from 4 to 4.2 mm), insonifies a volume of 53.74 mL.

## Field work

Data were extracted from 7 vertical profiles (18 347 image pairs) out of a total of 19 (42 779 total image pairs) profiles acquired during a cruise aboard *R/V New Horizon* on 28–29 March 2012 in the Southern California Bight at inshore (Scripps Canyon) and offshore (San Diego Trough) locations. A Conductivity-Temperature-Depth sensor (SBE 911 plus) equipped with a fluorometer (Seapoint Chlorophyll *a* Fluorometer) was mounted on the ZOOPS-O$^2$ platform for this fieldwork (Figure 1a). Maximum cast depths ranged between 40 and 500 m, the maximum operational depth of the package.

## Optical data analysis

### *Manual counting and identification of zooplankton and marine snow particles*

The ZOOPS-O$^2$ samples at 1 Hz, generating two still images and one acoustic record every second. To estimate the concentration of zooplankton and marine snow particles, we only used images from O-Cam 1. Using only one camera increases the likelihood of finding zooplankton and marine snow in the already small sampling volume of each camera (106 mL). The images from O-Cam 1 were manually processed by visually identifying and counting zooplankton and marine snow particles in each frame. For ease of processing and to save the data automatically to a disk, we used a custom-made point-and-click graphical user interface in MATLAB. Particles were sorted into 22 categories (e.g. euphausiids, calanoid copepods, jellyfish, marine snow, etc.). Concentration estimates (individuals per mL) for each category were obtained by dividing the number of organisms or particles per image by the camera's imaged volume.

### *Diatom-like particle semi-automatic image identification and quantification*

The ZOOPS-O$^2$ images were processed to identify the number of diatom-like particles and their 3D locations. The 3D location of each particle in the stereoscopic volume was estimated based on a careful stereo calibration of the cameras (see details in Briseño-Avena *et al.*, 2015). First, a subset of the images was used to construct a training set of diatom-like particles by manually selecting the objects identified as centric diatoms. In the images the centric diatoms were clearly distinguishable as circular opaque objects when viewed end-on, and in side view both thecae (Petri dish-like shape) were obvious. Then, some descriptors of the manually selected objects were obtained using an automated image-processing algorithm. The algorithm automatically detects connected pixels [i.e. the object, or region of interest (ROI)] with a high contrast against the image background and extracts object descriptors such as location on the object in the image (centroid), size measurements (i.e. length or major axis, width or minor axis, area occupied by the pixels), and aspect ratio. This was implemented using "*regionprops*" in MATLAB's Image Processing Toolbox, but similar methods are available in other programming languages with similar image-processing toolboxes. Next, the descriptors for each ROI were used to automatically detect diatom-like particles in images from the O-Cam 1 and O-Cam 2 (Figure 2a and b). Visual inspection of at least 100 randomly selected image pairs corroborated that the automatic processing was accurate in identifying the centric diatoms. Finally, using the stereoscopic calibration described in Briseño-Avena *et al.* (2015), corresponding diatom-like particles found within the stereoscopic volume were identified from the image pairs (Figure 2a, open circles). That is, when particles in O-Cam 1 images (crosses) are

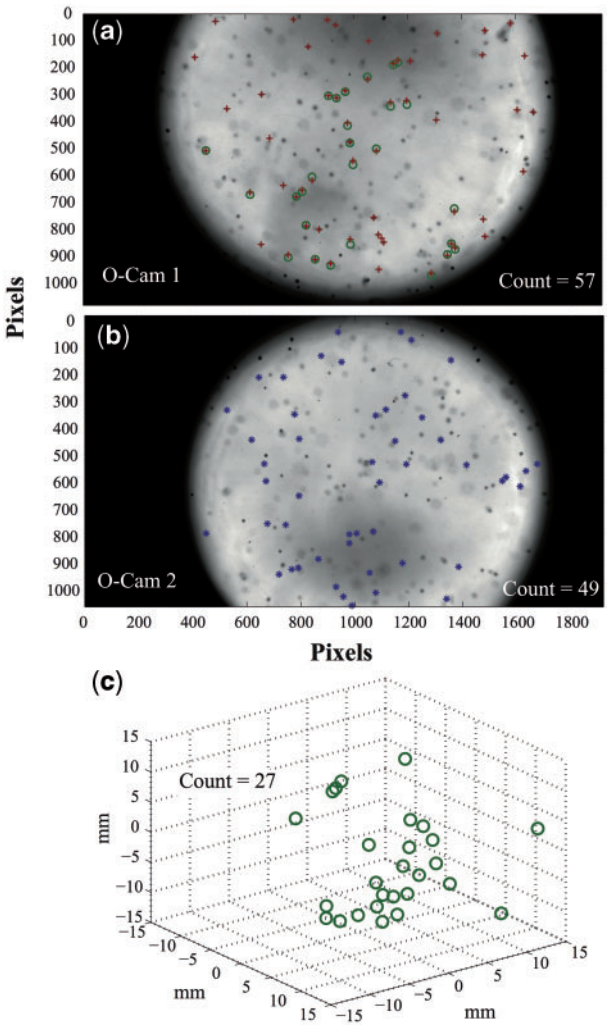


**Figure 2.** Result of the diatom-like particle detection. Images from the two O-Cams showing the automatic detection of diatom-like particles [crosses in (a) and stars in (b)]. Open circles that overlap the crosses in (a) indicate the diatom-like particles that have a corresponding particle in (b). Counts in (a) and (b) are the total numbers of diatom-like particles identified by the automatic detection algorithm. (c) Total diatom-like particles and their 3D locations in the stereoscopic volume.

overlapped by open circles, the algorithm has found the exact particles imaged by O-Cam 2 (Figure 2b, stars). The open circle also carries information of the predicted 3D coordinate of the particle imaged simultaneously by both cameras (Figure 2c). The remaining particles (black dots not marked in Figure 2a and b) were outside of this common stereoscopic volume and hence not quantified. Diatom-like particle concentration was then estimated by dividing the total diatom-like particle counts (Figure 2c) by the estimated stereoscopic imaged volume (~20.0 mL).

## Acoustic data analysis

### *Individual zooplankton and marine snow in situ acoustic reflections*

The 18 347 image pairs and their accompanying acoustic records were processed using the 'echo-locator' algorithm reported in Briseño-Avena *et al.* (2015). Briefly, the ZOOPS-O$^2$ stereoscopic volume intersected the acoustic beam at 0.84 and 0.88 m range; the acoustic records containing echoes (visualized as peaks in the echogram) within that range were extracted for further processing. These features mostly appeared as distinct, isolated peaks with BTS values at or above −120 dB. Next, the image pairs were viewed side-by-side along with their corresponding echogram. Once the identified acoustic target was confirmed to be in the stereoscopic volume, its acoustic range was estimated from the images. The projected acoustic range was then compared with that of the echogram: when the projected (optical) range of the echo matched the actual (acoustic) range of the location of the echo peak, we assumed that the echo originated from the stereoscopically imaged target. The echo properties (range, BTS, raw echo signal, and echo envelope) were saved for further analysis. The matching particles were then measured and their length was recorded. Table 1 summarizes the basic statistics.

## Comparing in situ BTS spectra to distorted wave born approximation spectra estimates

We computed the estimated spectra $B(f)$ from individual targets using the equation:

$$B(f) = 10log_{10}|\frac{CP_{bs}(f)}{CP_{sphere}(f)}|^2 - 58.1 \text{ dB } re \text{ 1 } m, \quad (2)$$

where $CP_{sphere}(f)$ is the Fourier transform of the windowed and zero-padded first reflection of the calibration sphere, and $CP_{bs}(f)$ the Fourier transform of the windowed and zero-padded echo from the target.

The DWBA (distorted wave born approximation) model (Chu and Ye, 1999; Briseño-Avena *et al.*, 2015) was applied to all targets using a prolate spheroid approximation after estimating the length ($L$), width ($W$), and orientation ($\theta$) of a target with respect to the transducer. This model requires values for density contrast ($g$) and sound-speed contrast ($h$). Because several previously poorly studied groups were included, values were taken from the literature (Greenlaw and Johnson, 1982; Chu and Wiebe, 2005; Smith *et al.*, 2010). Values of $g = 1.05$ and $h = 1.05$ were used for all developmental stages of copepods. For other taxa, the ($g$, $h$) values used were: (1.04, 1.022) for hydromedusae, (1.04, 1.07) for mysids, and (1.028, 1.022) for euphausiids. Groups for which no values were available in the literature (i.e. marine snow, appendicularians, siphonulae, doliolids, ctenophores, radiolarians, ostracods, and "others") were assigned values similar to these, based on our best judgment.

### *Acoustic concentration estimates of zooplankton and marine snow*

Field studies show that ZOOPS-O$^2$ is able to detect echoes from individual targets ranging in size from 360 µm to just under 2.5 cm (Table 1). Many of these echoes corresponded to visually identified individual zooplankton and marine snow particles. Particle/organism concentrations were estimated by counting the number of echoes (echo counting) recorded from ranges 0.65 to 1.22 m (full operational range of the system) and, dividing the total target counts by the effective acoustic beam volume (1 L).

### *Acoustic concentration estimates of diatom-like particles*

To test the ability of ZOOPS-O$^2$ to detect phytoplankton aggregated in high densities, the concentration estimates obtained from the automated diatom-like particle detection algorithm

**Table 1.** *In situ* BTS measured from individual targets using ZOOPS-O$^2$.

| Group | Sample size (*n*) | L (mm) | W (mm) | *a* (mm) | BTS (dB) |
|---|---|---|---|---|---|
| Copepods[a] | 224 | 0.35–4.5 | 0.02–1.2 | 0.04–0.8 | −113.9 to − 100.2 |
| Marine snow | 86 | 0.05–25 | 0.18–7 | 0.27–7.6 | −113.9 to − 105.5 |
| Euphausiids[b] | 2 | 4.6–4.7 | 0.48–0.52 | 0.95–1.1 | −113.0 to − 108.8 |
| Mysids | 4 | 1.6–6.5 | 0.35–0.55 | 0.31–0.63 | −108.3 to − 104.8 |
| Appendicularians[c] | 22 | 1.5–11.4 | 0.11–1.2 | 0.24–1.4 | −113.7 to − 105.0 |
| Chaetognaths | 3 | 7.8–15 | 0.66–0.76 | 0.75–1.0 | −114.5 to − 106.3 |
| Siphonulae[d] | 3 | 0.6–1.15 | 0.37–0.75 | 0.21–0.43 | −106.1 to − 105.0 |
| Hydromedusae | 8 | 0.7–3.7 | 2.1–19.6 | 0.95–3.2 | −113.9 to − 104.6 |
| Doliolids | 12 | 4.3–10.4 | 2.2–6.5 | 1.4–3.8 | −112.9 to − 105.5 |
| Ctenophore | 1 | 3.7 | 5.9 | 2.5 | −110.9 |
| Radiolarian | 1 | 1.8 | 1.9 | 0.95 | −111.1 |
| Ostracod | 1 | 1.3 | 0.44 | 0.31 | −110.0 |
| Others | 6 | 0.7–30 | 0.13–1.7 | 0.19–2.2 | −113.0 to − 104.3 |

Lengths (L) and widths (W) (mm) are stereoscopically derived measurements; the equivalent spherical radius (*a*) was estimated from the volume of a prolate spheroid of major (L/2) and minor (W/2) semi-axes.

[a]Mostly calanoid and poecilostomatoid copepods. It may include early developmental stages. Length of copepods is the estimated prosome length.

[b]Small euphausiids (probably juvenile stages).

[c]Including individuals with and without their "house".

[d]An early developmental stage of siphonophores.

described above were compared with the acoustic reflectivity profile. One profile, in which bulk fluorescence was dominated by centric diatoms (determined to be *Coscinodiscus* sp. from a water sample taken during the cruise), is used for this comparison. We assumed that diatoms had a reflectivity between −130 and −123 dB. Since no other zooplankton or marine snow particle returned such low BTS values, we interpreted any echoes within this 7 dB range as originating from the diatoms. The number of peaks (assumed to be individual diatoms) detected in this range interval was divided by the estimated acoustic volume (53.74 mL) of the beam between ranges 0.84 and 0.88 m (the range intercepted by the stereoscopic volume) to obtain acoustic estimates of diatom-like target concentration, reported here as targets per mL.

## Results and discussion

After rigorous examination and selection, only 373 image pairs (out of 18 347) clearly showed a single planktonic particle/organism common to both images, whose position also yielded an unambiguous echo in the acoustic record. From these image pairs we found a diverse group of *echogenic* targets (Table 1).

Values of *ka* (the product of the acoustic wave number *k* and the equivalent spherical radius *a*; Demer and Martin, 1995) at the centre frequency of ZOOPS-O$^2$ (2 MHz) were computed for all the targets identified in Table 1 (Figure 3). With the exception of two targets (small copepods; Figure 3a), all the individual targets were found to be located in the geometric scattering region ($ka > 1$). In no case was there a clear linear relationship between *ka* and BTS, suggesting that size (*a*) is not a good predictor of BTS at the centre frequency of the system. It is likely that other body properties (e.g. density, body shape, internal organs) have a stronger influence than size on the acoustic reflectivity of the organisms and marine snow studied in this work.

### Zooplankton and marine snow acoustic reflectivity

We obtained echoes from individual crustacean zooplankton (e.g. copepods, euphausiids, and mysids; Figure 4), but were surprised to find small gelatinous organisms (e.g. hydromedusae, doliolids, chaetognaths, appendicularians; Figure 5) and marine snow particles (Figure 6) in the acoustic records. Phytoplanktons were also present in the acoustic and stereoscopic records; we discuss this group separately below. Interestingly, we found that, despite the size range of the targets, there was a general overlap of BTS values for all categories (Table 1). These observations suggest that at frequencies of 1.5–2.5 MHz, and using only BTS, a large marine snow particle (Figure 6b) can return as much acoustic energy as—and be confounded with—small crustacean zooplankton (Figure 4). Although the size of the target has an impact on the scattered sound, the body or particle composition is also a large factor affecting the acoustic return. For instance, while the marine snow particle in Figure 6b is larger than the measured copepods, the marine snow is much more porous than the body of the crustacean. Thus its density and sound speed contrast properties would be much smaller, producing a weaker return than if it were a more compact, dense object. Although object orientation could also impact the acoustic return, at least for copepods, BTS was found to depend only weakly on orientation, with a mean difference between side and head-on views of only 7 dB (Briseño-Avena *et al.*, 2015).

Marine snow layers are common features in coastal oceans, yet their contribution to acoustic returns in field surveys seems to be virtually unexplored. Importantly, these layers can have intense biological activity. For example, the coincidence of marine snow layers, copepods, and their predators has been documented in the Baltic Sea using underwater optics (Möller *et al.*, 2012). In light of the present results, the collocation of such targets can complicate acoustic processing and interpretation, potentially leading to an over-estimate, e.g. of small crustacean abundance when acoustic returns from marine snow particles are mistaken for organisms.

Though the TS (dB) of some gelatinous organisms has been measured using narrowband, single frequency systems, most studies have focused on physonect siphonophores (a colonial pelagic cnidarian with a pneumatophore or "float", filled mostly with carbon monoxide): the air-filled pneumatophore strongly scatters sound. The TS of large jellyfish has also been measured using narrowband frequencies centered at 120 and 200 kHz (*Aurelia aurita*, umbrella diameter: 9.5–15.5 cm; Mutlu, 1996),

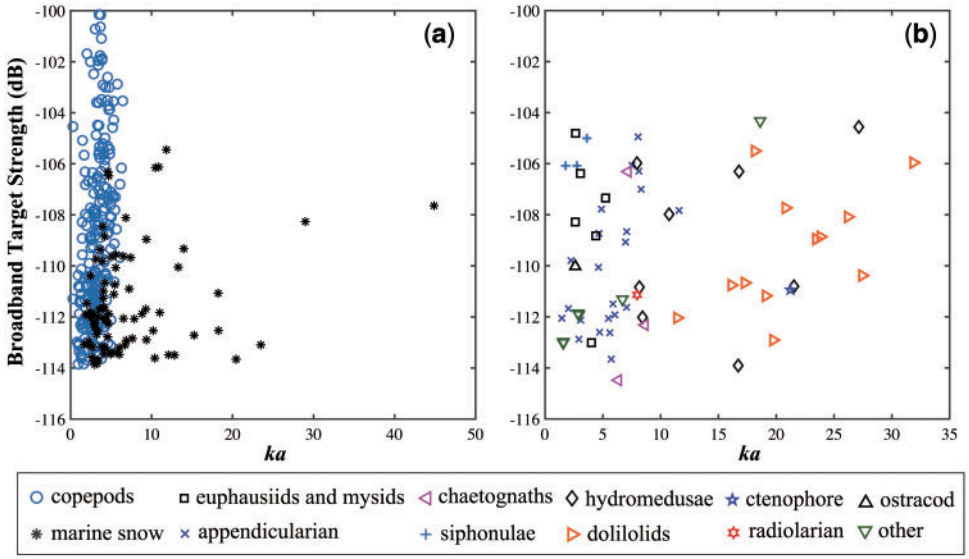


**Figure 3.** Summary of *ka* (wavenumber x equivalent spherical radius) vs. BTS for all targets reported in Table 1. Panel (a) copepods and marine snow. Panel (b) euphausiids, mysids, appendicularians, chaetognaths, siphonulae, hydromedusae, doliolids, ctenophore, radiolarian, ostracod, and other. The wavenumber was estimated at the system centre frequency of 2 MHz.

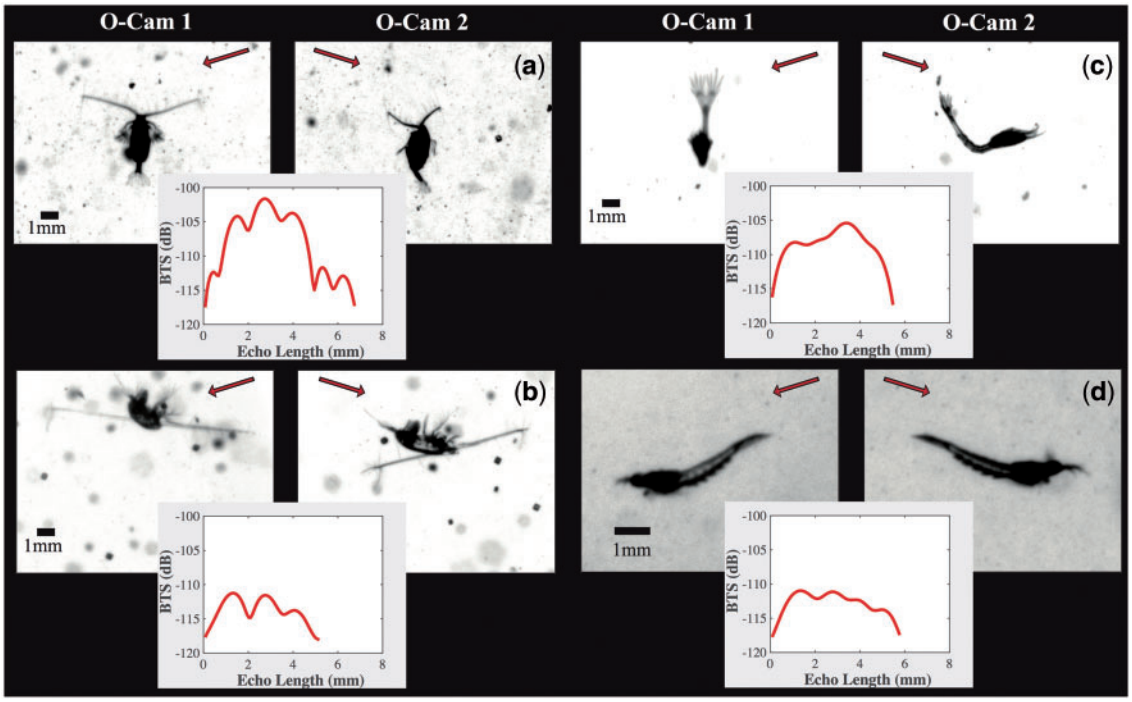


**Figure 4.** Examples of individual crustacean zooplankton whose BTS (in dB) was measured *in situ* with ZOOPS-O$^2$. For each triplet: left image = O-Cam 1, right image = O-Cam 2, overlapping plot = echo envelope (solid line). Scale bars are given for each image pair. The arrows indicate the direction of the incident acoustic waves. (a) Calanoid copepod; (b) Eucalanid copepod; (c) Mysid; (d) Euphausiid.

and at 18, 38, and 120 kHz (*Chrysaora hysoscella* (5–8.5 cm), *Aequorea aequorea* (10–61 cm); Brierley *et al.*, 2005, and *Chrysaora melanaster* (21–31 cm); De Robertis and Taylor, 2014). The hydromedusae measured in the present study were much smaller, ranging from 0.2 to 2.4 cm bell diameter. Notice that at frequencies of 1.5-2.5 MHz, the BTS of a large gelatinous organism (Figure 5a) could be misinterpreted as a medium-sized copepod (Figure 4a). However, the shape of the echo envelope (Figures 4 and 5, red lines on overlapping plots) is qualitatively different for these two groups, although the orientation of a target in relation to the direction of the incident acoustic wave may affect the echo envelope shape. At present, however, only measurements related to the TS (or BTS as in this work) of targets are generally utilized in the acoustic community. The properties of

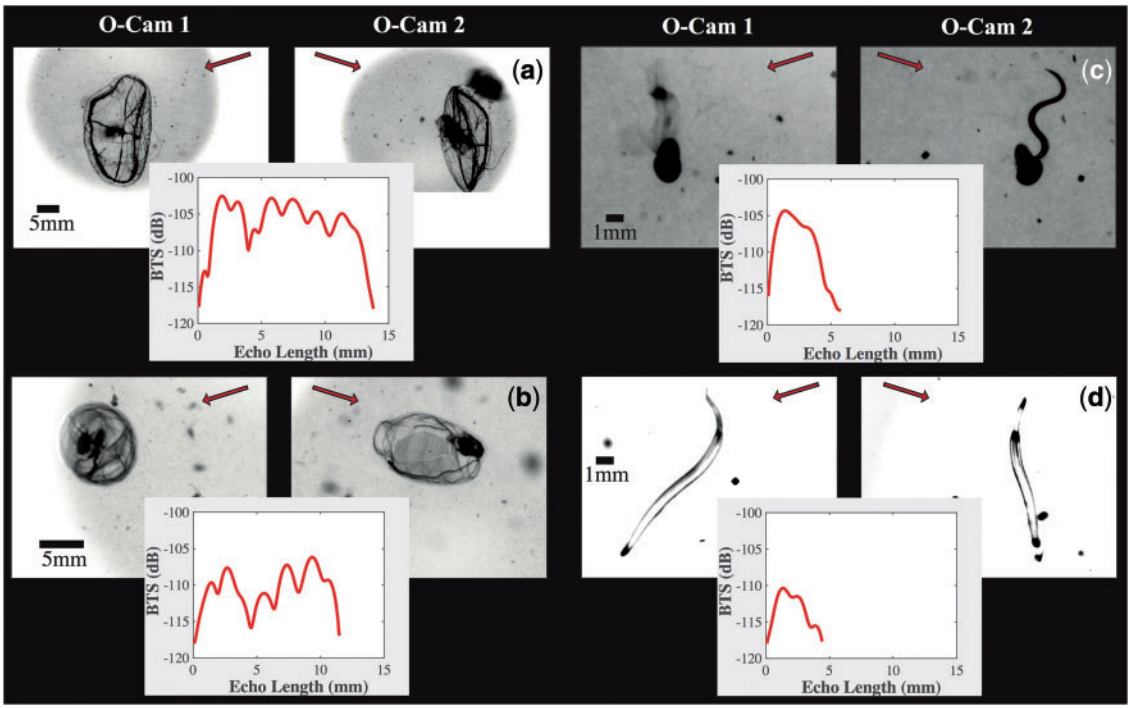


**Figure 5.** Examples of individual gelatinous and other fragile zooplankton whose BTS (in dB) was measured *in situ* with ZOOPS-O$^2$. Legend same as Figure 4. (a) Hydromedusa; (b) Doliolid; (c) Appendicularian; (d) Chaetognath.

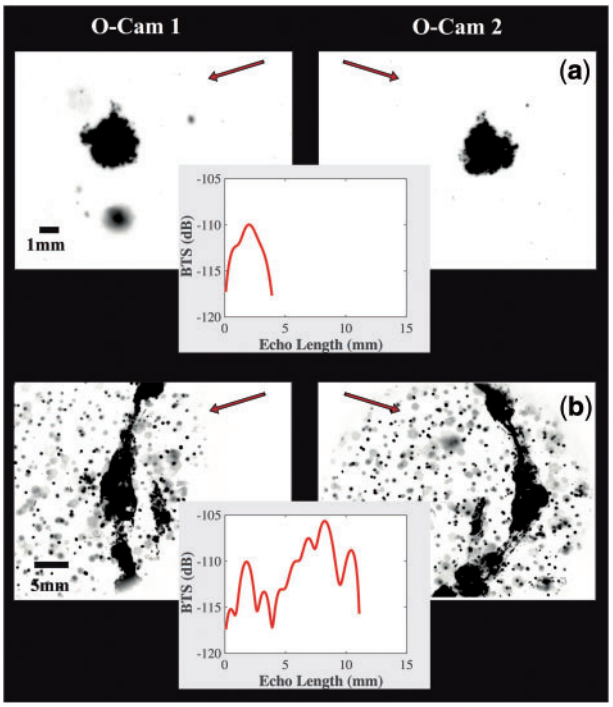


**Figure 6.** Examples of small (a) and large (b) marine snow particles whose BTS (in dB) was measured *in situ* with ZOOPS-O$^2$. Legend same as Figure 4.

the echo envelope related to each individual target should be investigated in future work, such as has been done with fish (e.g. Reeder and Stanton, 2004). This work is a cautionary tale for interpreting acoustic data from emerging broadband, high frequency technologies—and even more significantly, single, narrowband technologies—that rely on echo-integrating principles. As we have shown, many unexpected taxa have the potential to contribute to acoustic signals.

### *DWBA model vs. BTS spectra measurements*

As part of our research effort we also sought to examine the agreement of a well-known model, the DWBA, with our collected data. The comparison of measured [$B(f)$] and modelled (DWBA) spectra yielded interesting results (Figure 7) for a copepod, euphausiid, mysid, large crustacean carcass, doliolid, hydromedusa, and large and small marine snow particles. Our DWBA model yielded spectra comparable to the measured spectra; though the nulls do not always match up, they are in close agreement. The peak BTS values (Figure 7, stars) for each individual are plotted (arbitrarily centered on the x axis): a single TS value does not vary among groups as much as the spectra do. Notice that the euphausiid's measured and modelled spectra (Figure 7b) had the greatest discrepancy in magnitude; one likely factor is that the $g$ and $h$ values available in the literature were often for animals larger than the ones we observed. Another factor is the simplicity of our model compared with the actual shape of the organism or relative to the bent cylinder and higher resolution models of Stanton and Chu (2000) where orientation, as well as material properties (i.e. $g$ and $h$) are identified as important factors affecting the TS from individual euphausiids.

To explore how the results from the high-frequencies used by ZOOPS-O$^2$ would apply to more commonly used frequencies in acoustic surveys we extended our DWBA model to include frequencies from 38 kHz to 2.5 MHz. For each measured and modelled target we then located the frequency of the transition from geometric to Rayleigh (G-R) scattering (Figure 8). For most

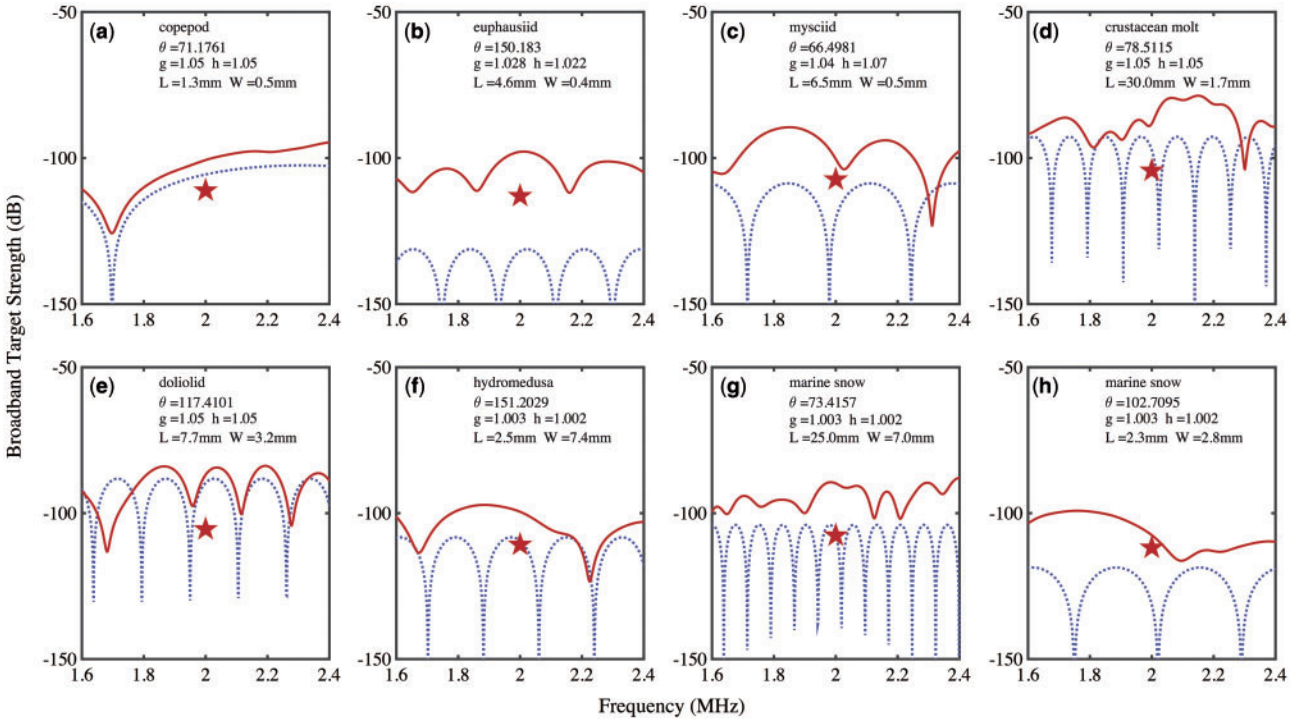


**Figure 7.** Measured ($B(f)$, solid lines) and modelled (DWBA, dotted lines) spectra, and target BTS (stars) from eight targets at different orientations with respect to the sonar. Different values of $g$ and $h$ where used for different groups, and they are noted in each panel. The values of $\theta$ are given in degrees. L, length (major axis a); W, width (minor axis b).

organisms, including the appendicularian shown in Figure 8a, the mean G-R transition frequency is located within the range of commonly used lower frequencies (shaded area and downward-pointing triangles in Figure 8b). Most systems using lower frequencies than ZOOPS-$O^2$ measure volume backscatter strength rather than individual echoes and direct comparisons between measurements are not recommended. However, the fact that the G-R transitions for the particles and organisms reported here occur at frequencies between 38 and 420 kHz suggests that the results from this high-frequency, broadband system might apply to the more commonly used lower-frequency narrowband systems when such particles and organisms are found in high concentrations or dense aggregations.

## Phytoplankton acoustic reflectivity

To explore whether diatoms found at the deep chlorophyll *a* maximum in high densities (e.g. those observed in thin layers) reflect sound we used a profile with a well-defined peak as shown by the bulk fluorescence signal (Figure 9a and b). A water sample taken at the depth of the chlorophyll maximum and later inspected under a microscope confirmed that the phytoplankton assemblage was comprised of the centric diatom *Coscinodiscus* sp.: one of the largest solitary marine planktonic genera, measuring up to 500 µm in diameter in 250 µm in width, similar in size to the ones imaged by the O-cams. At the centre frequency of the system (2 MHz) such large diatoms have a $ka = 1.5$ (i.e. $ka > 1$), suggesting that they are detectable by the ZOOPS if their sound speed and density contrast are high enough. We refer to these imaged centric diatoms as "diatom-like particles" due to limitations of the image processing method utilized. However, no other phytoplankton types were apparent in the image records; suggesting the layer was dominated by a single species. The maxima in concentration of these diatom-like particles peaked in the same depth interval as the fluorescence, suggesting that these diatoms dominated the fluorescence signal (Figure 9b). Stereoscopically derived concentration estimates of the centric diatoms (Figure 9c, thick dashed line) fall within the range observed in the Southern California Bight region (e.g. Venrick, 2012). We found an increase in the acoustic-derived concentration of targets with BTS values between −130 and −123 dB coincident with both the diatom-like concentration peaks and the layer of high-intensity bulk fluorescence. This observation provides support for the hypothesis that these large diatoms were the source of the acoustic signal.

Dense phytoplankton aggregations are often regions of intense grazing, and increased abundances of zooplankton within or near the observed diatom peaks might be expected. However, acoustic- and optic-derived concentration estimates of zooplankton (targets whose BTS > −120 dB; Table 1) and marine snow are comparable in magnitude through the entire profile (Figure 9c, thin solid line and dotted line, respectively), and their concentrations did *not* peak with the diatoms concentrations. This suggested that neither zooplankton nor marine snow were the cause of the increased acoustic signals found within the diatom peaks (Figure 9c, thick solid line). This further supported the hypothesis that the high concentration of diatoms was responsible for the broadband, high-frequency (1.5–2.5 MHz) signal detected by the ZOOPS-$O^2$ system.

One other potential source of the acoustic signal in the layers is thermal microstructure. Acoustic scattering associated with the thermocline, e.g. was reported as early as Weston (1958). It has also been found that thermal structures are sensed by broadband systems at

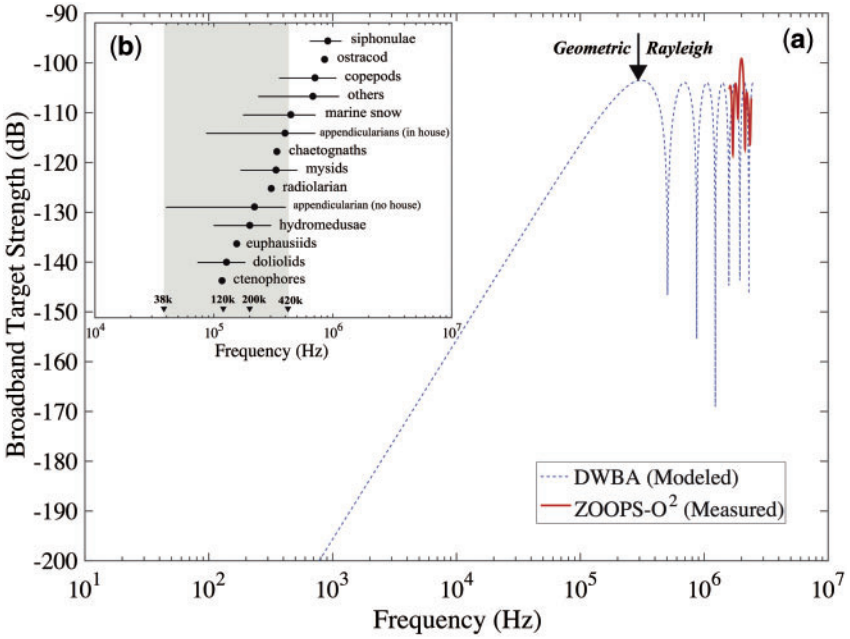


**Figure 8.** G-R transition location for modelled (DWBA) spectra. (a) Example of the G-R location (downward-pointing arrow) on the modelled spectrum (dotted line) of an appendicularian (inside its house) using a fluid-like prolate spheroid of L = 3.7 mm, W = 0.8 mm, $\theta$ = 120°, $g$ = 1.05, and $h$ = 1.05. The corresponding *in situ* measured spectrum is superimposed (solid line). Inset (b): average (solid circles) ± 1 SD (horizontal lines) of the estimated G-R location for each group reported in Table 1. Shaded area encompasses the range of frequencies most commonly used by narrowband systems (downward-pointing triangles).

high and ultra-high frequencies (Holliday and Pieper, 1980; Lavery *et al.*, 2010). The coincidence of biological and thermal structures has been recognized since early acoustic underwater research (Gessner, 1948; Cushing *et al.*, 1956; Cushing and Richardson, 1956; Tveite, 1969; Derenbach *et al.*, 1980). Given that ZOOPS-O$^2$ is a broadband system operating at 1.5–2.5 MHz, we wanted to rule out the possibility that the acoustic signal in the profile in Figure 9c (thick solid line) was due to thermal microstructure.

To test this, temperature, acoustic and stereoscopically derived diatom-like concentration data were binned over 1 meter, and temperature gradients estimated by measuring the change in temperature ($dT$) over 1 m depth ($dZ$) bins (Figure 10, thin black solid line). Three main sharp temperature gradients were apparent. The first (Figure 10, feature labelled "1") was found above the diatom peaks, and the two subsequent ones (Figure 10, features labelled "2" and "3") at the top and bottom of the two diatom-like peaks. If the increase in the acoustic signal (Figures 9c and 10, thick solid line) was solely a response to the sharp temperature gradients, one would expect to see three corresponding acoustic peaks. However, the acoustic signal did not drop where there were no sharp temperature gradients. Instead, high concentrations of diatom-like particles were observed in that depth interval. This suggested that temperature microstructure was not the main source of the observed acoustic return in the −130 to −123 dB signal. Furthermore, a simple regression showed that variations in the acoustic data were better explained by the stereoscopic (optically derived) diatom-like concentration ($r^2 = 0.85$) than by thermal gradients ($r^2 < 0.07$). Although this does not rule out the possibility of thermal microstructure contributing to some degree to the acoustic signal, our analyses suggest that the increase in the acoustic returns is primarily due to the presence of centric diatoms.

Interestingly, the relationship between the optic- and acoustic-derived densities of diatom-like particles was not linear (Figure 9c, inset). This suggests that at high diatom concentrations the acoustic signal became saturated, no longer reflecting the echoes of individual diatoms, but rather integrating over multiple targets. Because the diatoms were smaller than the range resolution (1.5 mm) of the sonar system, and multiple cells occurred in the volume at the same acoustic ranges, our system was not able to resolve echoes from individual phytoplankton cells at high concentrations. We did not pursue volume backscatter relationships in this article, and they remain a topic for further study. It is also apparent that the acoustically derived concentrations of diatom-like particles (Figure 10, thick solid line) are over estimated at lower concentrations (from camera estimates; dashed line). There are two explanations for why this might be happening. The first has to do with a signal to noise ratio (SNR) issue: because our estimates were near the lower threshold of our system for detecting individual echoes, it is possible that a low SNR might be preventing us from accurately estimating diatom abundance with the sonar. The second reason is the potential variability in diatom size through the profile. *Coscinodiscus* (the imaged diatoms reported in this work) range in diameter from 300 to 500 µm in diameter and 150–250 µm in width. At the lower size range ($a$ = 0.108 mm) these diatoms would have $ka$ = 0.9, effectively putting them in the Rayleigh scattering region ($ka < 1$). At the other end of the size range (and similar to the ones we encountered), *Coscinodiscus* has an equivalent spherical diameter of $a$ = 0.1802 and $ka$ = 1.5 (i.e. $ka > 1$; geometric region). Such variability in size might have also contributed to missing echoes from individual cells. It is not clear how much acoustic energy several small diatoms would reflect when in high concentrations. However, this work is not intended to show that the sonar is able to quantify diatom concentrations with the

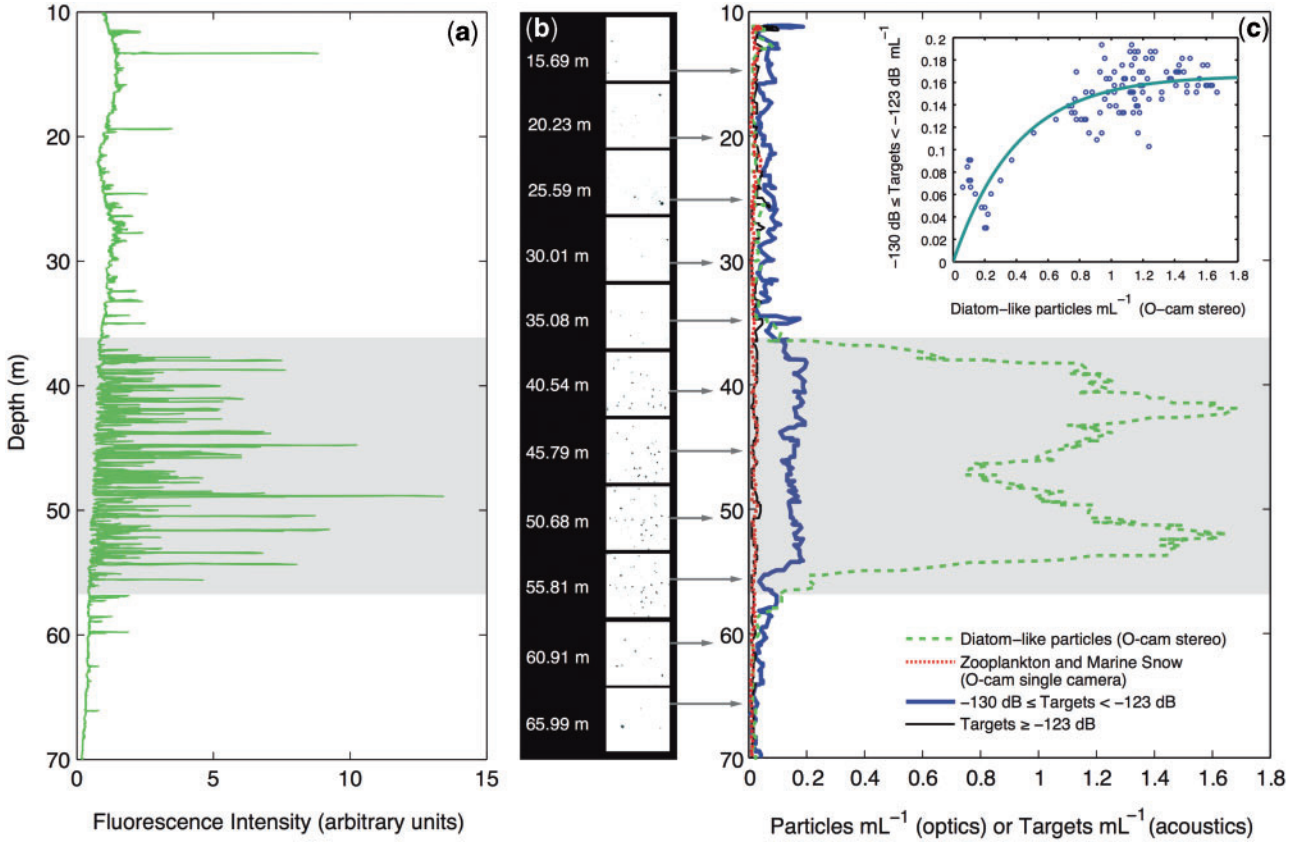


**Figure 9.** Acoustic reflections from two peaks of large centric diatoms sampled on 28 March 2012. (a) Fluorescence intensity profile; (b) images from O-Cam 1; (c) ZOOPS-O$^2$ profiles comparing optic (broken lines) and acoustic (solid lines) data; thin solid line represents targets in the range of zooplankton and marine snow (BTS $>-123$ dB); dotted line represents zooplankton and marine snow counts from one O-Cam; thick solid line indicates concentration estimates from acoustic data from targets whose BTS ranged between $-130$ and $-123$ dB (diatom-like targets); thick dashed line represents diatom-like particle concentration obtained with the semi-automatic quantification method. Inset in (c) shows the relationship between optically and acoustically derived estimates of diatom concentration.

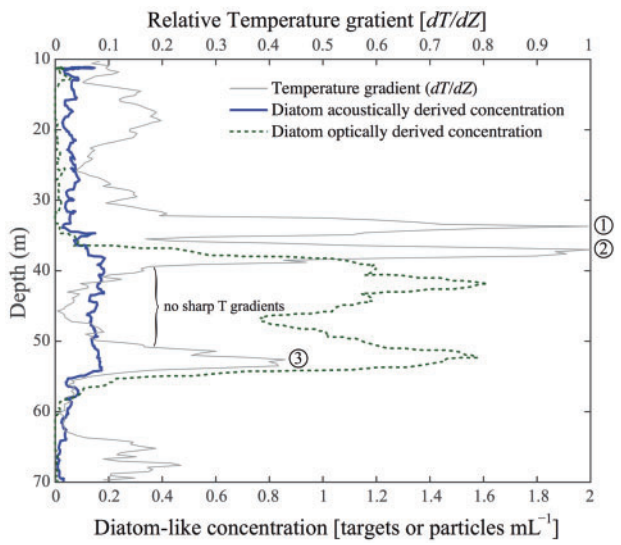


**Figure 10.** Optically and acoustically derived diatom-like concentrations (dashed line and thick solid line, respectively) and temperature gradients ($dT/dZ$; thin gray solid line) for the same profile shown in Figure 9. The three sharpest gradients in temperature are indicated with circled numbers 1, 2, and 3.

same accuracy as the optical method, but rather, to show that our sonar can record a measurable echo originating from locally high concentrations of diatom cells.

## Conclusions

In this work we have shown that individual gelatinous zooplankton and marine snow targets are capable of reflecting broadband, ultra high-frequency (1.5–2.5 MHz) acoustic energy. We also showed that layers of locally high diatom concentrations were capable of reflecting sound at these high frequencies. Knowing that diatom and marine snow layers are conspicuous and recurrent features in coastal areas, this work suggests that such particles should be taken into account during acoustic surveys, especially when high frequencies are used and the relative concentration of such particles is significantly higher than co-occurring zooplankton. Furthermore, gelatinous organisms (e.g. jellyfish, siphonophores, doliolids, and salps—although no salps where observed in this work) can dominate zooplankton communities at times (e.g. Richardson *et al.*, 2009; Everett *et al.*, 2011; Alvarez Colombo *et al.*, 2009) and can become significant contributors to acoustic signals, as it has been shown for the large jellyfish *C. melanaster* (De Robertis and Taylor, 2014).

It is hard to know whether the observations made with this broadband, high-frequency system are relevant to the more

commonly used lower-frequency systems without having empirical data. However, Figure 8b shows that the location for the transition frequency between the geometric and Rayleigh scattering in the modelled spectra for the type and size of targets observed here fall within the frequency range 38–420 kHz, and are therefore likely to be picked up by systems using these lower frequencies. These organisms could include large phytoplankton cells and phytoplankton chains; it is advisable, therefore, to exercise caution when interpreting narrowband acoustic data acquired in regions where large aggregations of phytoplankton or marine snow occur. For example, Timmerman *et al.* (2014) suggested that a layer composed of diatom flocculates was detected with a narrowband sonar using 200 kHz. Furthermore, it has been shown that phytoplankton-derived flocculates can carry bubbles (Riebesell, 1992), which can have a large resonance at lower frequencies than those considered in this work.

The emergence of commercially available broadband technologies creates new opportunities for the use of processing methods for interpreting acoustic data. Although not fully considered in this work, the properties of acoustic echoes (e.g. the echo envelope; lines in Figures 4–6) can add more information for acoustic target classification. The results presented here underscore the need to exercise caution when interpreting acoustic data based solely on TS measurements. This issue is particularly relevant when encountering a diverse group of *echogenic* particles that range widely in size but return overlapping BTS values (Table 1). Take for instance the case of copepods and doliolids: the tiny crustaceans can be an order of magnitude smaller than the pelagic tunicates, yet the measured BTS values overlapped significantly, despite of having no overlap in their *ka* values (Figure 3a and b).

Simple modelled spectra for organisms such as copepods, euphausiids, mysids, doliolids, and hydromedusae, as well as marine snow showed good agreement with *in situ* measurements. These results could be particular useful for models considering more complex body shapes, and organisms of different composition. The DWBA model using a prolate spheroid of dimensions similar to the organisms studied here could be used initially to aid in differentiation among targets. However, the relatively scarcity of *g* and *h* values for zooplankton hinders our ability to obtain more accurate comparisons. Given the sensitivity of the DWBA model to *g* and *h* (data not shown), we should strive to get better values for zooplankton to produce more accurate model results. In theory, one could diagnose *g* and *h* values by fitting model spectra to the measured spectra by varying *g* and *h*.

The work presented here may prove useful in biological field surveys; when possible, incorporating a suite of technologies including acoustic, optical imaging, and net systems will generate a more complete picture of planktonic distributions and possible insights to processes occurring at fine scales. In light of the present observations, it is advisable that zooplankton surveys using high-frequency acoustics take into account phytoplankton and marine snow, if such features are known to be conspicuous in the region studied. Although nets target a finite size-range of planktonic organisms—retaining large particles and destroying fragile organisms and marine snow particles—optical cameras are an important complement because of their non-invasive, non-destructive capabilities. Furthermore, nets cannot resolve the fine spatial scales at which phytoplankton and marine snow layers occur. Optical tools, on the other hand, can be used to detect such ubiquitous features and provide accurate ground truthing information for acoustic studies that might be affected by phytoplankton, marine snow and fragile, gelatinous taxa.

## Acknowledgements

We would like to thank the National Science Foundation (0728305) for funding the development of the ZOOPS-$O^2$ system. Christian Briseño-Avena would like to thank UC MEXUS (USA) and CONACyT (Mexico) for their support to fund his PhD studies at UC San Diego, Scripps Institution of Oceanography. We would also like to thank the captain and crew of the *R/V New Horizon* for their assistance during fieldwork. The authors thank three reviewers for their constructive criticism, which they found very helpful and resulted in an improved document.

## References

Alldredge, A. L., Cowles, T. J., MacIntyre, S., Rines, J. E. B., Donaghay, P. L., Greenlaw, C. F., Holliday, D. V. *et al.* 2002. Occurrence and mechanisms of formation of a dramatic thin layer of marine snow in a shallow Pacific fjord. Marine Ecology Progress Series, 233: 1–12.

Alldredge, A. L., and Silver, M. W. 1988. Characteristics, dynamics and significance of marine snow. Progress in Oceanography, 20: 41–82.

Alvarez Colombo, G., Benovic, A., Malej, A., Lucic, D., Makovec, T., Omofri, V., Acha, M. *et al.* 2009. Acoustic survey of a jellyfish-dominated ecosystem (Mljet Island, Croatia). In Pitt, K.A., and Purcell, J.E. (eds.) Jellyfish Blooms: Causes, Consequences, and Recent Advances. Developments in Hydrobiology, 206: 99–111.

Anoshkin, A. F., and Goncharov, V. K. 1993. Submersible vehicle investigation of sound scattering layers and hypotheses about their physical nature. Acoustical Physics, 39: 302–306.

Benfield, M. C., Wiebe, P. H., Stanton, T. K., Davis, C. S., Gallager, S. M., and Greene, C. H. 1998. Estimating the spatial distribution of zooplankton biomass by combining Video Plankton Recorder and single-frequency acoustic data. Deep-Sea Research II, 45: 1175–1199.

Bok, T., Na, J., and Paeng, D. 2013. Diel variation in high frequency acoustic backscatter from *Cochlodinium polykrikoides*. Journal of the Acoustic Society of America, 134: EL140–EL146.

Bok, T., Paeng, D., Na, J., and Kang, D. 2010. Ultrasound backscatter power from *Cochlodinium polykrikoides*, the main red tide species in the Southern Sea of Korea. Journal of Plankton Research, 32: 503–514.

Brierley, A. S., Boyer, D. C., Axelsen, B. E., Lynam, C. P., Sparks, C. A. J., Boyer, H. J., and Gibbons, M. J. 2005. Towards the acoustic estimation of jellyfish abundance. Marine Ecology Progress Series, 295: 105–111.

Briseño-Avena, C., Roberts, P. L. D., Franks, J. S. P., and Jaffe, J. S. 2015. ZOOPS-$O^2$: A broadband echosounder with coordinated stereo optical imaging for observing plankton *in situ*. Methods in Oceanography, 12: 36–54.

Chu, D., and Wiebe, P. H. 2005. Measurements of sound-speed and density contrasts of zooplankton in Antarctic waters. ICES Journal of Marine Science, 62: 818–831.

Chu, D., and Ye, Z. 1999. A phase-compensated distorted wave Born approximation representation of the bistatic scattering by weakly scattering objects: Application to zooplankton. Journal of the Acoustical Society of America, 106: 1732–1743.

Cowles, T. J., Desiderio, R. A., and Carr, M. 1998. Small-scale planktonic structure: persistence and trophic consequences. Oceanography, 11: 4–9.

Cushing, D. H., and Richardson, I. D. 1956. A record of plankton on the echo-sounder. Journal of the Marine Biological Association of the United Kingdom, 35: 231–240.

Cushing, D. H., Lee, A. J., and Richardson, I. D. 1956. Echo traces associated with thermonclines. ICES Journal of Marine Research, 15: 1–13.

Demer, D. A., and Martin, L. V. 1995. Zooplankton target strength: Volumetric or areal dependence? Journal of the Acoustical Society of America, 98: 1111–1118.

De Monte, S., Soccodato, A., Alvain, S., and d'Ovidio, F. 2013. Can we detect oceanic biodiversity hotspots from space? International Society for Microbial Ecology, 7: 2054–2056.

De Robertis, A., and Taylor, K. 2014. *In situ* target strength measurements of the scyphomedusa *Chrysaora melanaster*. Fisheries Oceanography, 153: 18–23.

Derenbach, J. B., Astheimer, H., Hansen, H. P., and Leach, H. 1979. Vertical microscale distribution of phytoplankton in relation to the thermocline. Marine Ecology Progress Series, 1: 187–193.

Everett, J. D., Baird, M. E., and Suthers, I. M. 2011. Three-dimensional structure of a swarm of the salp *Thalia democratica* within a cold-core eddy off southeast Australia. Journal of Geophysical Research, 116: C12046.

Fernandes, P. G., Gerlotto, F., Holliday, D. V., Nakken, O., and Simmonds, E. J. 2002. Acoustic applications in fisheries science: the ICES contribution. ICES Marine Science Symposia, 213: 483–492.

Fielding, S., Griffiths, G., and Roe, H. S. J. 2004. The biological validation of ADCP acoustic backscatter through direct comparison with net samples and model predictions based on acoustic-scattering models. ICES Journal of Marine Science, 61: 184–200.

Fornshell, J. A., and Tesei, A. 2013. The development of SONAR as a tool in marine biological research in the twentieth century. International Journal of Oceanography 2013: 1–9.

Gessner, F. 1948. The vertical distribution of phytoplankton and the thermocline. Ecology, 29: 386–389.

Greenlaw, F. C. 1977. Backscattering spectra of preserved zooplankton. Journal of the Acoustical Society of America, 62: 44–52.

Greenlaw, C. F., and Johnson, R. K. 1982. Physical and acoustical properties of zooplankton. Journal of the Acoustical Society of America, 72: 1706–1710.

Holliday, D. V., and Pieper, R. E. 1980. Volume scattering strengths and zooplankton distributions at acoustic frequencies between 0.5 and 3 MHz. Journal of the Acoustical Society of America, 67: 135–146.

Jaffe, J. S., Ohman, M. D., and De Robertis, A. 1998. OASIS in the sea: measurement of the acoustic reflectivity of zooplankton with concurrent optical imaging. Deep-Sea Research II, 45: 1239–1253.

Lara-Lopez, A., and Neira, F. J. 2008. Synchronicity between zooplantkton biomass and larval fish concentrations along a highly flushed Tasmanian estuary: assessment using net and acoustic methods. Journal of Plankton Research, 30: 1061–1073.

Lavery, A. C., Chu, D., and Moum, J. N. 2010. Measurements of acoustic scattering from zooplankton and oceanic microstructure using a broadband echosounder. ICES Journal of Marine Science, 67: 379–394.

Lawson, G. L., Wiebe, P. H., Ashjian, C. J., Gallager, S. M., Davis, C. S., and Warren, J. D. 2004. Acoustically-inferred zooplankton distribution in relation to hydrography west of the Antarctic Peninsula. Deep-Sea Research II, 51: 2041–2072.

Martin, L. V., Stanton, T. K., Wiebe, P. H., and Lynch, J. F. 1996. Acoustic classification of zooplankton. ICES Journal of Marine Science, 53: 217–224.

McManus, M. A., Alldredge, A. L., Barnard, A. H., Boss, E., Case, J. F., Cowles, T. J., Donaghay, P. L. *et al.* 2003. Characteristics, distribution and persistence of thin layers over a 48 hour period. Marine Ecology Progress Series, 261: 1–19.

Möller, K. O., St. John, M., Temming, A., Floeter, J., Sell, A. F., Herrmann, J., and Möllmann, C. 2012. Marine snow, zooplankton and thin layers: indications of a trophic link from small-scale sampling with the Video Plankton Recorder. Marine Ecology Progress Series, 468: 57–69.

Mutlu, E. 1996. Target strength of the common jellyfish (*Aurelia aurita*): a preliminary experimental study with a dual-beam acoustic system. ICES Journal of Marine Science, 53: 309–311.

Powell, J. R., and Ohman, M. D. 2012. Use of glider-class acoustic Doppler profilers for estimating zooplankton biomass. Journal of Plankton Research, 34: 563–568.

Ransom, B., Shea, K. F., Burkett, P. J., Bennet, R. H., and Baerwald, R. 1998. Comparison of pelagic and nepheloid layer marine snow: implications for carbon cycling. Marine Geology, 150: 39–50.

Reeder, D. B., and Stanton, T. K. 2004. Acoustic scattering by axisymmetric finite-length bodies: An extension of a two-dimensional conformal mapping method. Journal of the Acoustical Society of America, 116: 729–746.

Richardson, A. J., Bakun, A., Hays, G. C., and Gibbons, M. J. 2009. The jellyfish joyride: causes, consequences and management responses to a more gelatinous future. Trends in Ecology and Evolution, 24: 312–322.

Richter, K. E. 1984. Acoustic scattering at 1.2 MHz from individual zooplankters and copepod populations. Deep-Sea Research, 32: 149–161.

Riebesell, U. 1992. The formation of large marine snow and its sustained residence in surface waters. Limnology and Oceanography, 37: 63–76.

Selivanovsky, D. A., Stunzhas, P. A., and Didenkulov, I. N. 1996. Acoustical investigation of phytoplankton. ICES Journal of Marine Science, 53: 313–316.

Smith, J. N., Ressler, P. H., and Warren, J. D. 2010. Material properties of euphausiids and other zooplankton from the Bering Sea. Journal of the Acoustical Society of America, 128: 2664–2680.

Stanton, T. K. 2012. 30 years of advances in active bioacoustics: A personal perspective. Methods in Oceanography, 1–2: 49–77.

Stanton, T. K., and Chu, D. 2000. Review and recommendations for the modeling of acoustic scattering by fluid-like elongated zooplankton: euphausiids and copepods. ICES Journal of Marine Science, 57: 793–807.

Stanton, T. K., Chu, D., and Wiebe, P. H. 1996. Acoustic scattering characteristics of several zooplankton groups. ICES Journal of Marine Science, 53: 289–295.

Sutor, M., Cowles, T. J., Peterson, W., and Lamb, J. 2005. Comparison of acoustic and net sampling systems to determine patterns in zooplankton distributions. Journal of Geophysical Research, 110: C10S16.

Timmerman, A. H. V., McManus, M. A., Cheriton, O. M., Cowen, R. K., Greer, A. T., Kudela, R. M., Ruttenberg, K. *et al.* 2014. Hidden thin layers of toxic diatoms in a coastal bay. Deep-Sea Research II, 101: 129–140.

Trenkel, V. M., Handegard, N. O., and Weber, T. C. 2016. Observing the ocean interior in support of integrated management. ICES Journal of Marine Science, 73: 1947–1954.

Tveite, S. 1969. Zooplankton and the discontinuity layer in relation to echo traces in the Oslofjord. Fiskeridirektoratets Skrifter Serie Havundersoekelser, 15: 25–35.

Venrick, E. L. 2012. Phytoplankton in the California Current system off southern California: Changes in a changing environment. Progress in Oceanography, 104: 46–58.

Warren, J. D., and Smith, J. N. 2007. Density and sound speed of two gelatinous zooplankton: Ctenophore (*Mnemiopsis leidyi*) and lion's mane jellyfish (*Cyanea capillata*). Journal of the Acoustic Society of America, 122: 574–580.

Weston, D. E. 1958. Observations on a scattering layer at the thermocline. Deep-Sea Research, 5: 44–50.

Wiebe, P. H., Chu, D., Kaartvedt, S., Hundt, A., Melle, W., Ona, E., and Batta-Lona, P. 2010. The acoustic properties of Salpa thompsoni. ICES Journal of Marine Science, 67: 583–593.

Wiebe, P. H., Mountain, D. G., Stanton, T. K., Greene, C. H., Lough, G., Kaartvedt, S., Dawson, J., and Copley, N. 1996. Acoustical study of the spatial distribution of plankton on Georges Bank and the relationship between volume backscattering strength and the taxonomic composition of the plankton. Deep-Sea Research II, 43: 1971–2001.

*Handling editor: Howard Browman*